Supporting Information. Self-assembly of Amphiphilic Polyelectrolytes in Trivalent Salt

Liyan Liu, Fujia Wang, Xinyi Liu, Lide Guo, Xiujun Gao, and Hongge Tan

1 Simulation Section

1.1 Simulation Method:

A shifted and truncated Lennard-Jones (LJ) potential is used to describe the van der Waals interactions between any two beads

$$U_{LJ}\left(r_{ij}\right)=\begin{cases}4\varepsilon_{LJ}\left[\left(\frac{\sigma}{r_{ij}}\right)^{12}-\left(\frac{\sigma}{r_{ij}}\right)^{6}-\left(\frac{\sigma}{r_c}\right)^{12}+\left(\frac{\sigma}{r_c}\right)^{6}\right] & r_{ij}<r_c\\ 0 & r_{ij}>r_c\end{cases} \quad (2)$$

where ε_{LJ} represents the strength of pairwise interaction, and r_c is the cutoff radius. For the interactions between the polymer beads with the same type, the cutoff distances are r_c=2.5σ, and the strength of pairwise interaction ε_{LJ} are $2.0k_BT$ at room temperature $T=298K$ (k_B is the Boltzmann constant) for the hydrophobic beads and $0.2k_BT$ for the hydrophilic PE beads. The interactions between the polymer monomers of the same type model different implicit solvent quality for the copolymer blocks.[3] For all other pairs of beads, the parameters of r_c and ε_{LJ} are $2^{1/6}\sigma$ and $1.0k_BT$, respectively, to represent fully repulsive interactions. All particles are modeled as spherical beads with the same diameter σ regardless of the particle type for simplicity.

The neighboring chain beads are connected by the finitely extensible nonlinear elastic (FENE) potential

$$U_{bond}(r_{ij})=-\frac{1}{2}kR^2{}_0\ln\left[1-\left(\frac{r_{ij}}{R_0}\right)^2\right] \quad (1)$$

in which k=$30k_BT/\sigma$ and R_0=1.5σ are the spring constant and the maximum bond length, respectively,[1, 2] and r_{ij} is the distance between the i-th and j-th beads.

Coulomb potential is used to describe the electrostatic interactions between any two charged particles q_i and q_j

$$U_{Coul}(r_{ij})=k_BT\frac{\lambda_B q_i q_j}{r_{ij}} \quad (3)$$

where λ_B is Bjerrum length, $\lambda_B=e^2/\left(4\pi\varepsilon_0\varepsilon_r k_BT\right)$, which is defined as the distance at which the electrostatic energy of two basic charges is equal to the thermal energy k_BT. The solvent is a continuous dielectric medium and is treated implicitly, and ε_0 and ε_r are the permittivity of vacuum and the relative dielectric constant of the solvent, respectively. The Bjerrum length is set as λ_B=3.0σ. [4] In water and at room temperature, ε_r=80 and λ_B=7.1Å, and therefore σ=2.4Å. Coulomb long-range interactions are calculated by the particle-particle/particle-mesh (PPPM)

[5]algorithm with an estimated accuracy of 10^{-3}.

A constant temperature T^*=1.0 (which corresponds to 298K, $T^*=T/\varepsilon_{LJ}$) is maintained by coupling the system to a Langvin thermostat. The motion of particle is described by Langvin equation

$$m\frac{d^2\vec{r}_i(t)}{dt^2} = -\nabla U_i - \xi\frac{d\vec{r}_i(t)}{dt} + \vec{F}_i^R(t) \tag{4}$$

where m is the mass of the particle, U_i is the total potential, ξ and $\vec{F}_i^R(t)$ are the friction coefficient and stochastic force with a zero average value. In this paper, the standard LJ units (mass m, length σ and energy ε_{LJ}) are used to represent all physical quantities. The value of ξ is set to $\xi = 1.0\tau^{-1}$, where $\tau = \sigma\left(m/\varepsilon_{LJ}\right)^{1/2}$. The motion of beads is solved by velocity-Verlet algorithm, and the value of integration time step is set as $\Delta t = 0.005\tau$. Initially, a fully repulsive LJ potential is applied to obtain a random distribution of copolymer chains and salt ions. Then, the system is equilibrated for 2.0×10^7 steps until the time evolution of thermodynamic quantities and the radius of gyration of copolymer chains reach a stable state regime. After the equilibrium run, another 4.0×10^6 steps are performed in the production run. During the production, data from the simulation are saved every 2.0×10^4 steps for analysis.

1.2 The radii of gyration as functions of time

The radii of gyration of hydrophilic and hydrophobic blocks obtained from the three independent replicas as functions of time at different salt contents are plotted in Figure S1, respectively. It clearly shows that the radii of gyration converged after equilibrating 2.0×10^7 steps (the $2.0\times10^7 th$ step corresponds to the point with the value of 200 on the time axis), and they are consistent with each other in the production run.

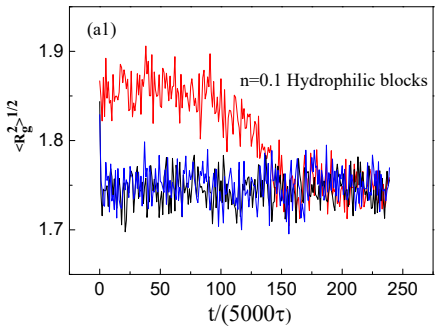

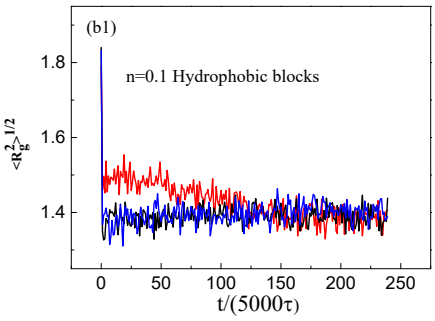

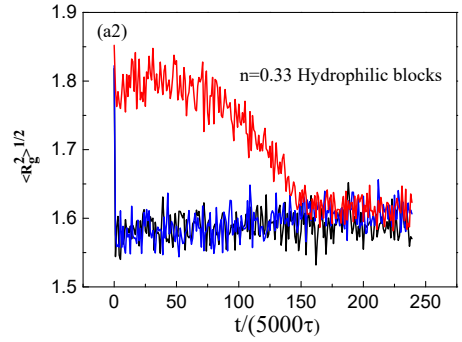
(a2)
n=0.33 Hydrophilic blocks
$\langle R_g^2 \rangle^{1/2}$
t/(5000τ)

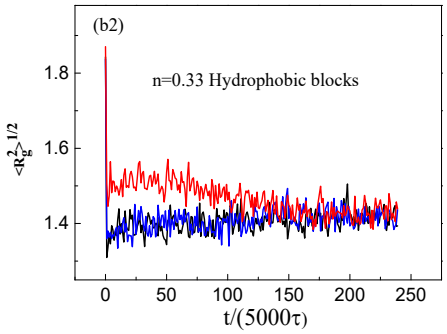
(b2)
n=0.33 Hydrophobic blocks
$\langle R_g^2 \rangle^{1/2}$
t/(5000τ)

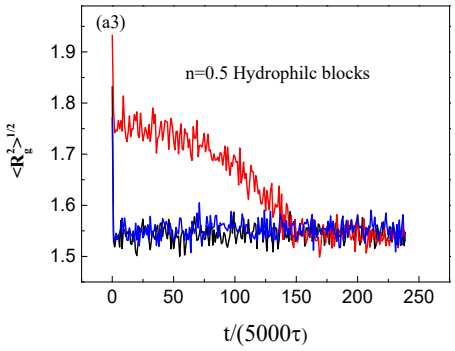
(a3)
n=0.5 Hydrophilc blocks
$\langle R_g^2 \rangle^{1/2}$
t/(5000τ)

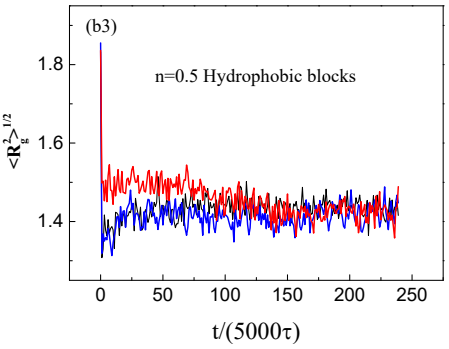
(b3)
n=0.5 Hydrophobic blocks
$\langle R_g^2 \rangle^{1/2}$
t/(5000τ)

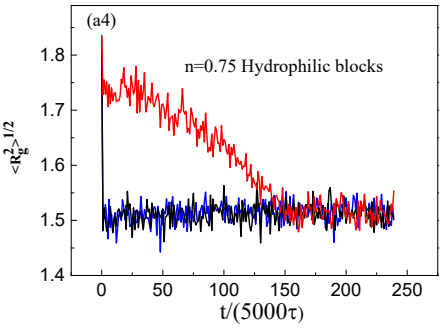
(a4)
n=0.75 Hydrophilic blocks
$\langle R_g^2 \rangle^{1/2}$
t/(5000τ)

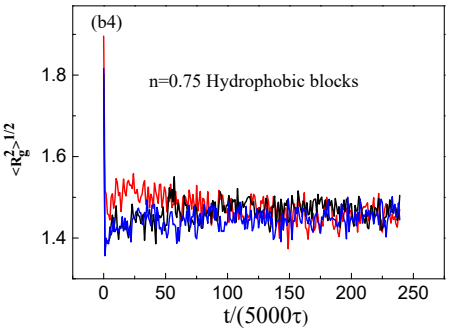
(b4)
n=0.75 Hydrophobic blocks
$\langle R_g^2 \rangle^{1/2}$
t/(5000τ)

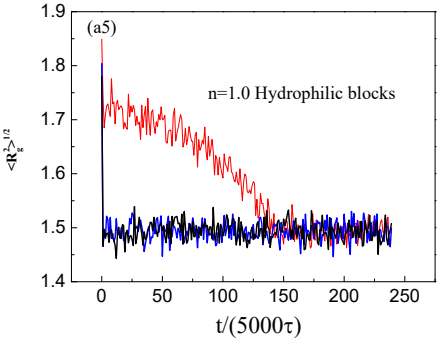
(a5)
n=1.0 Hydrophilic blocks
$\langle R_g^2 \rangle^{1/2}$
t/(5000τ)

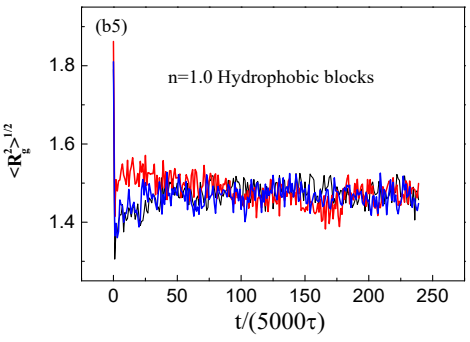
(b5)
n=1.0 Hydrophobic blocks
$\langle R_g^2 \rangle^{1/2}$
t/(5000τ)

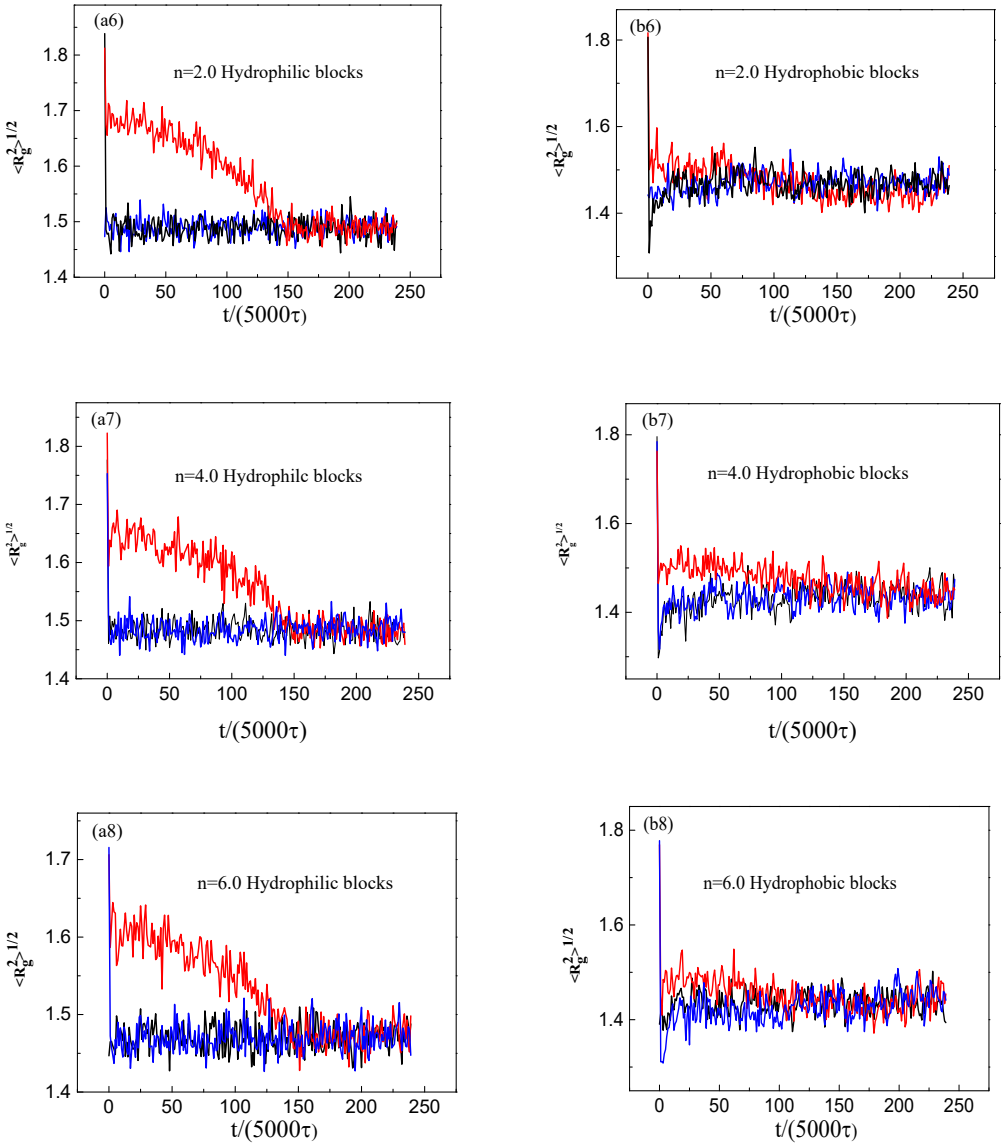

Figure S1. The radii of gyration of hydrophilic and hydrophobic blocks as functions of time obtained from three independent replicas are plotted. The radii of gyration obtained from the replica starts at a higher temperature are shown by red, and from the other two replicas are shown by black and blue, respectively.

1.3. Time-averaged density profiles on x-z and y-z planes

Time-averaged top-down views of PE monomers (left panels), monovalent (middle panels) and trivalent counterions (right panels) density profiles on x-z and y-z planes are demonstrated in Figure S2 and S3, respectively.

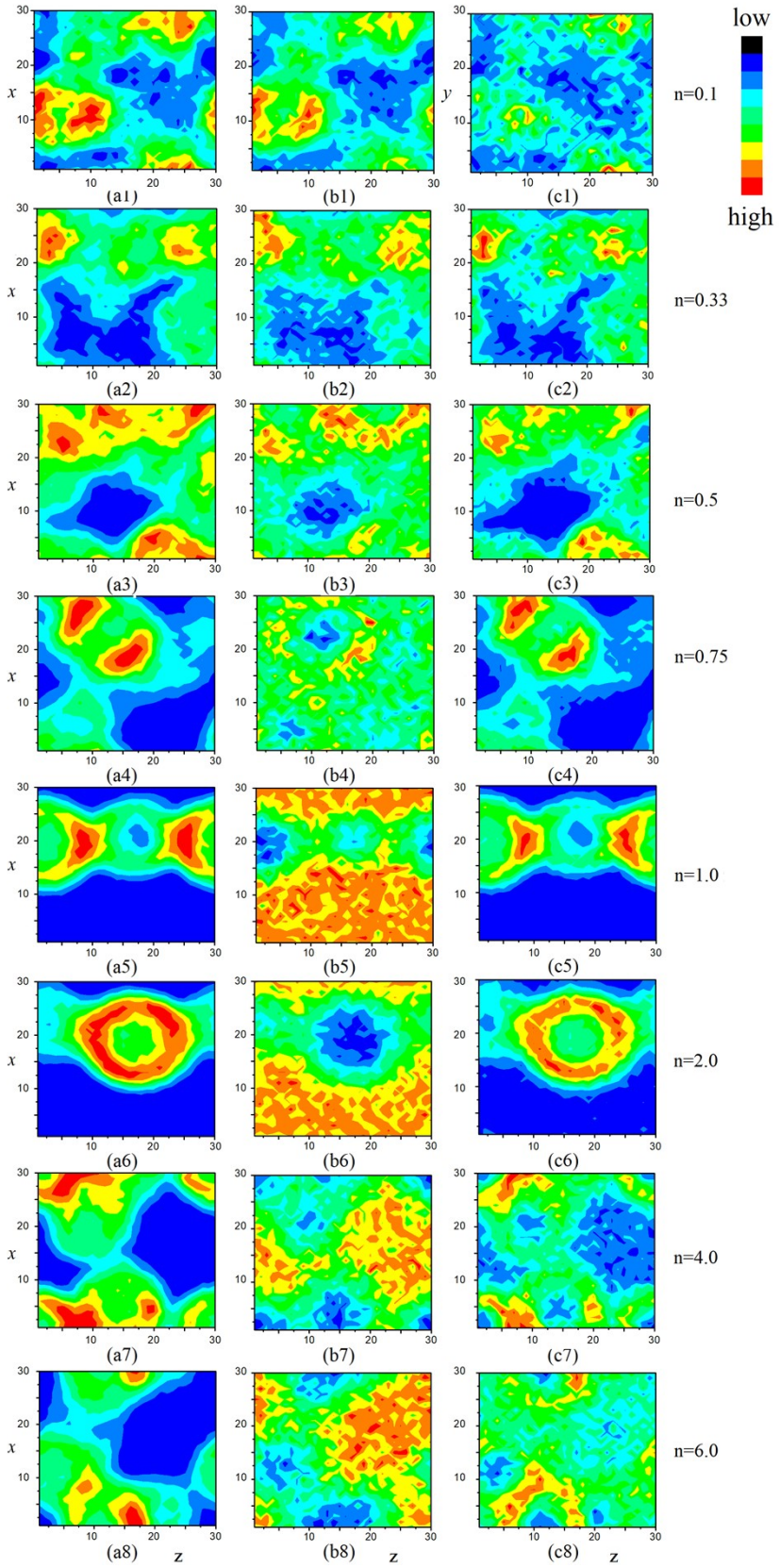

Figure S2. Local density distributions of PE monomers (left panels), monovalent counterions (middle panels) and trivalent counterions (right panels) on x-z plane (top-down view) at different salt concentrations. Color scale corresponds to relative particle densities (red for high density, dark blue for low density), with relative densities scaled to the lowest value in each image.

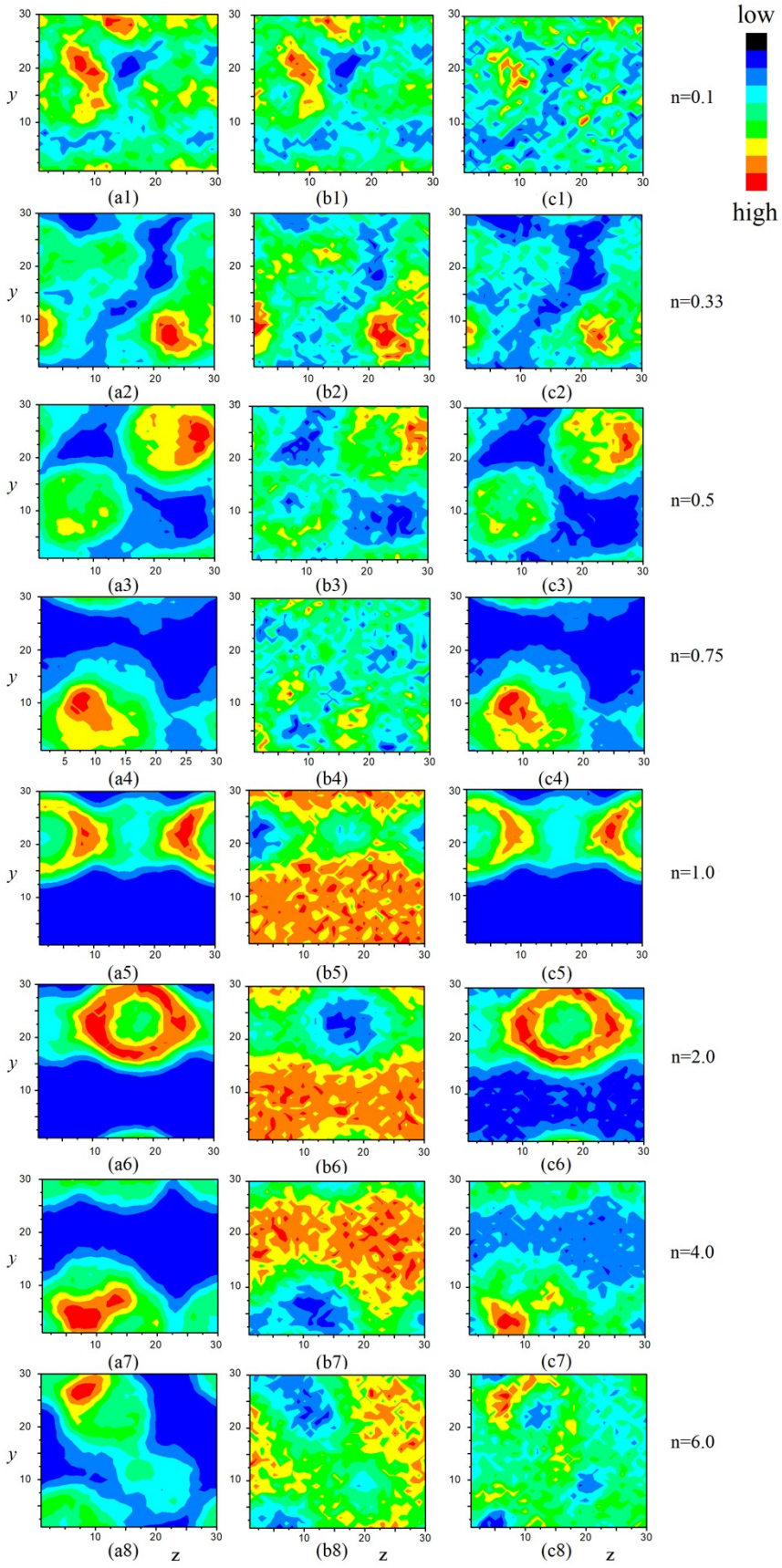

Figure S3. Local density distributions of PE monomers (left panels), monovalent counterions (middle panels)

and trivalent counterions (right panels) on y-z plane (top-down view) at different salt concentrations. Color scale corresponds to relative particle densities (red for high density, dark blue for low density), with relative densities scaled to the lowest value in each image.

1.4 Time-averaged density profiles of micelles at different salt contents

Time-averaged density profiles of micelles at different salt concentrations are shown in Figure S4.

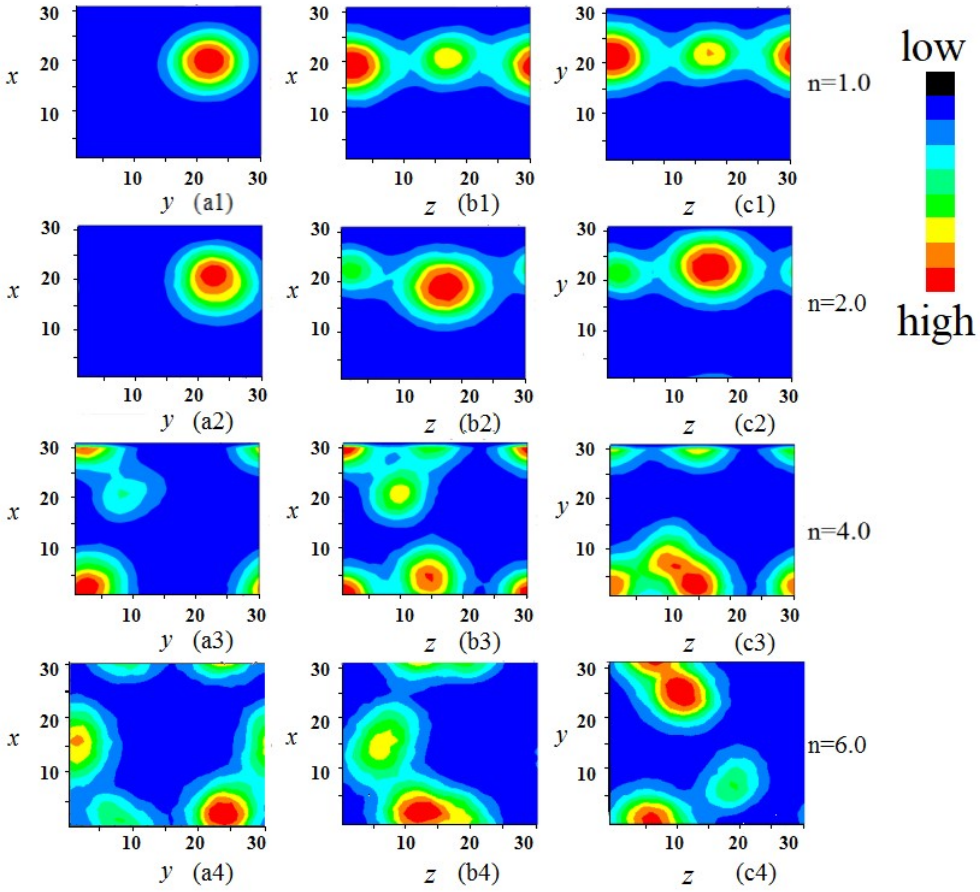

Figure S4. Time-averaged density profiles of the assembled micelles on x-y plane (left panels), x-z plane (middle panels) and y-z plane (right panels) at different salt concentrations. Color scale corresponds to relative particle densities (red for high density, dark blue for low density), with relative densities scaled to the lowest value in each image.

1.5 Reentrant transition of the assemble micelles

Time-averaged density profiles of the assembled micelles at ρ=0.03σ^{-3} at different salt concentrations are shown in Figure S5, which clearly demonstrate the four states of the assembled micelles in reentrant behavior.

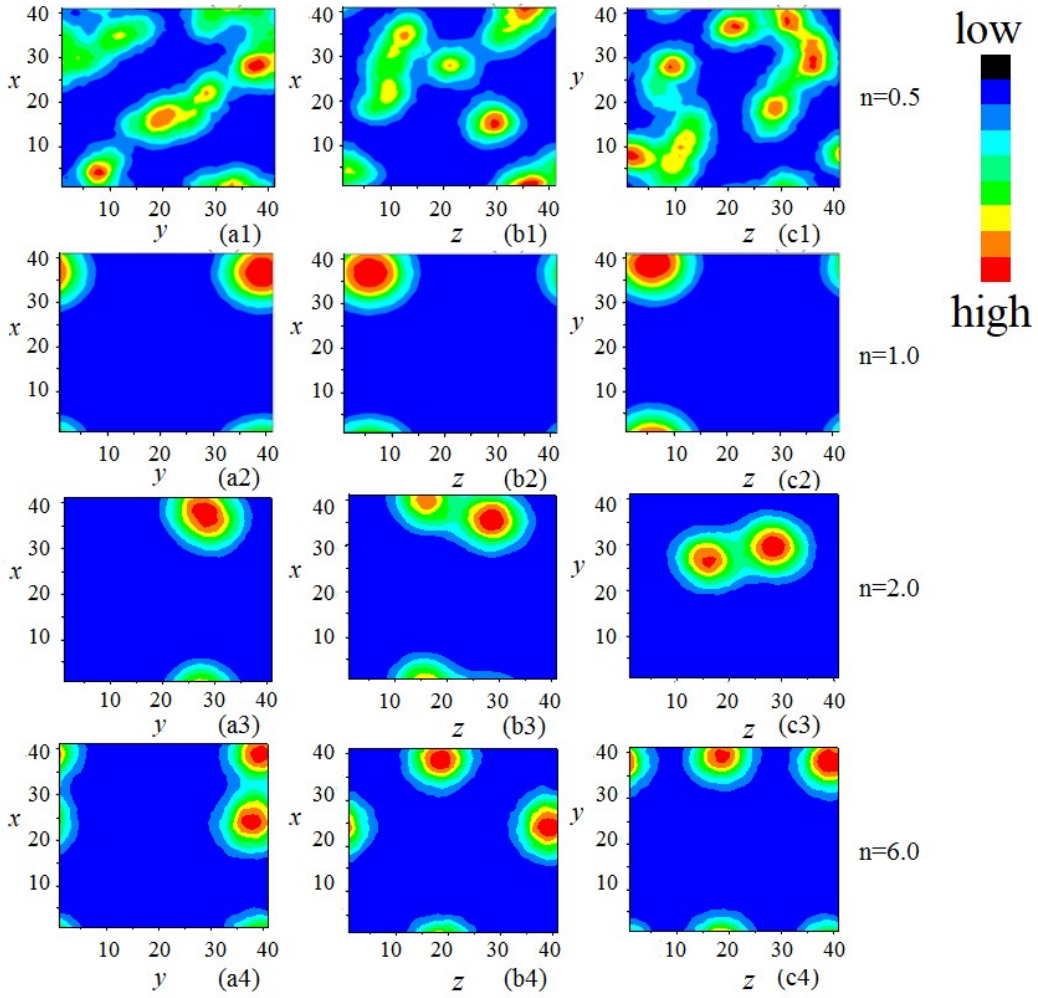

Figure S5. Time averaged density profiles of the assembled micelles on x-y plane (left panels), x-z plane (middle panels) and y-z plane (right panels) at different salt contents. Color scale corresponds to relative particle densities (red for high density, dark blue for low density), with relative densities scaled to the lowest value in each image.

1.6 Time-averaged density profiles of micelles at different polymer densities

Time-averaged density profiles of the assembled micelles at different polymer densities are shown in Figure S6.

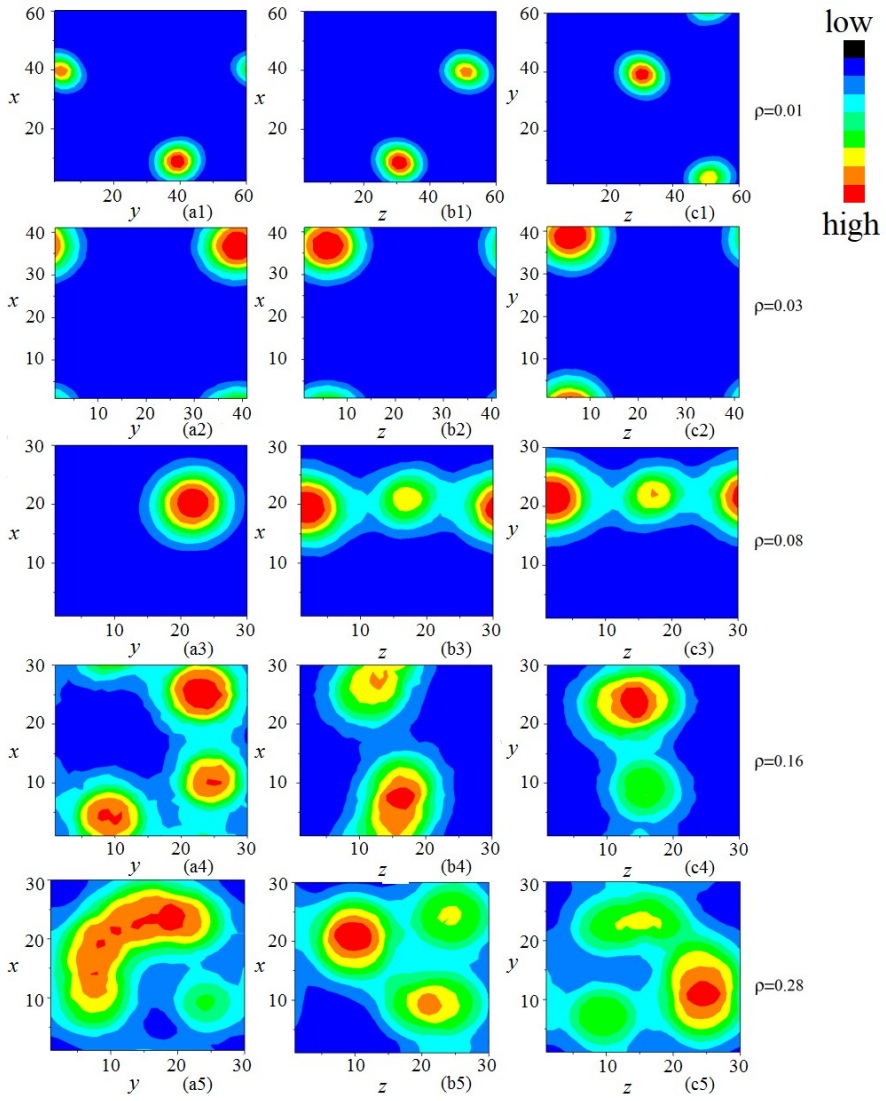

Figure S6. Time-averaged density profiles of PE copolymers on x-y plane (left panels), x-z plane (middle panels) and y-z plane (right panels) at different polymer concentrations. Color scale corresponds to relative particle densities (red for high density, dark blue for low density), with relative densities scaled to the lowest value in each image.

2 Experimentation Section

2.1 Materials

1-Ethyl-3-(3-dimethyllamino-propyl), carbodiimide (EDC), N-Hydroxysuccinimide (NHS), 4-dime-thylaminopyridine (DMAP), Dimethyl sulfide (DMSO), Aluminium chloride ($AlCl_3$), D2O, DMSO-d_6, Molecular sieves types 4A were purchased from Bohua Reagent Co., Ltd. (Tianjin, China), Ethyl ether, Hydrogen chloride (HCl), Polyaspartic acid (PASP, molecular weight 8-12 kDa) were purchased from Huaxia Reagent Co., Ltd. (Sichuan,China),

poly(lactic-co-glycolic acid)(PLGA, molecular weight 10kDa) were purchased from Daigang Biomaterial Co., Ltd. (Jinan, China). All other organic solvents and reagents were purchased from commercial sources and were used as received unless otherwise stated.

2.2 Preparation of materials

Poly (lactic-co-glycolic acid)-Polyaspartic acid (PLGA-PASP) was synthesized by a typical

amide reaction. 0.05mmol PLGA (0.5 g) was dissolved in 10ml dewatered DMSO. After PLGA was completely dissolved, 0.2 mmol EDC (0.031g) and 0.15 mmol NHS (0.017g) were added, heated to 45 degrees for 12 hours under N_2. 2 ml hydrochloric acid (0.1 M) was used to terminate EDC, 0.05mmol PASP (0.4 g) and 0.005 mmol of DMAP (0.006g) were added and stirred for 12 hours at 45 degrees. The solution was poured into 40 ml anhydrous ethanol and centrifuged at room temperature at 8000 rpm for 10 minutes. The precipitation was washed by ethanol and double distilled water twice. The product was obtained by freeze-drying. The structure was characterized by ^{1}H nuclear magnetic resonance (^{1}H NMR) as shown in Figure S7. The molecular weight and the polydispersity of PLGA-PASP were measured by gel permeation chromatography (GPC) as shown in Table S1.

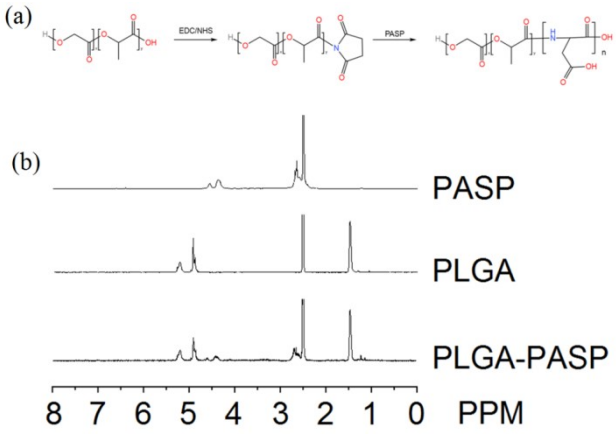

Figure S7. Synthesis and structure characterization by ^{1}H NMR of PLGA-PASP.

Table S1. GPC results of PLGA-PASP.

Materials	Molecular weight (kDa)	PDI	Yield (%)
PLGA-PASP	21.3	1.2	54.5%

2.3 Construction of micelles

Micelles were composed from PLGA-PASP and prepared by nanoprecipitation method. PLGA-PASP was dissolved in 1 mL of DMSO, slowly added into 9 mL of ion solution in distilled water with vigorous stirring. The micelles were then transferred into dialysis bags (cutoff 50 KDa) and dialyzed for 8 hours in different concentrations of aluminium chloride. The pH of micelles was 5.6. The pKa of PASP is 5.1. The degree of ionization of COOH of PASP was calculated by the following equation

$$pH=pKa+lg(COO^-/COOH) \quad (5)$$

In order to verify the presences of the chain-like and planar supra-micellar structures predicted by MD simulations, two different concentrations of PLGA-PASP solution were prepared. In simulations, the polymer density at which planar aggregation of micelles occurs was twice of that chain-like association, the same concentration ratio was retained in experiment. The content of $AlCl_3$ in solution was calculated through eq. (1) to be at n=1.0, keeping consistent with simulation conditions. The detailed information was shown in Table S2.

Table S2. Construction conditions of PLGA-PASP Micelles.

Concentrations of PLGA-PASP (mmol/L)	Concentrations of $AlCl_3$ (mmol/L)	Zeta potential (mV)
0.0020	0.0000	-14.4±0.96
0.0020	0.0005	18.47±1.80
0.0040	0.0010	17.63±2.39

2.4 Morphology of PLGA-PASP in aluminium chloride solution

Different morphologies of diblock PLGA-PASP micelles in aluminum chloride solution were formed, which were characterized by transmission electron microscope (TEM, Philips EM400ST). Briefly, a drop of micelles was placed onto a 200 mesh copper grid and allowed to equilibrate. Following deposition of Micelles, water was removed from the grids with a filter paper at room temperature. The mesh copper grid was vacuum dried before being loaded in the microscope.

Chain-like and planar aggregations of the assembled micelles predicted by simulation results were confirmed by experiments. Diblock PLGA-PASP spherical micelles were obtained. The spherical micelles then aggregated into micron sized polymer chains and planar networks. A long polymer chain and planar networks of inter-connected micelles were clearly demonstrated in TEM images in Figure S8 (a) and (b), respectively. The images in Figure 3 (b) and Figure 10 (b) corresponded to the marked areas in Figure S8 (a) and (b), respectively.

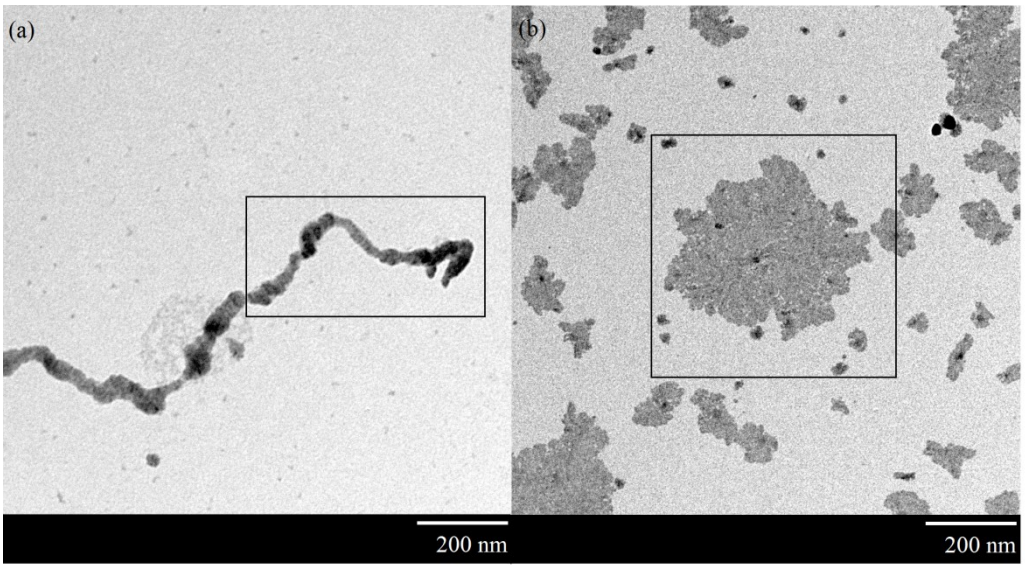

Figure S8. TEM images of PLGA-PASP micelles. The concentration of PLGA-PASP is 0.002 mmol/L (a) and 0.004 mmol/L (b), respectively.

TEM images of the micelles without and with trivalent salt before dialysis at the concentration of PLGA-PASP 0.002 mmol/L were shown in Fig. S9 (a) and (b), respectively. The addition of trivalent salt led to a sharp reduction in micelle size, as cleraly demonstrated by the TEM images, which mightbe mainly attributed to the following two reasons. The first one was the effect of electrostatic interactions. The charged PASP were stretched under the electristatic repulsions. With the addition of trivalent salt, the strong electrostatic attractions between trivalent counterions and PASP effectively reduced the repulsions, and the bridging of trivalent ions may induce the folding of PASP chains. The second one was related to hydration of the micelles. The

water spread out of the micelles by the effect of osmotic pressure in the salt solution, which also shrinked the micelles.

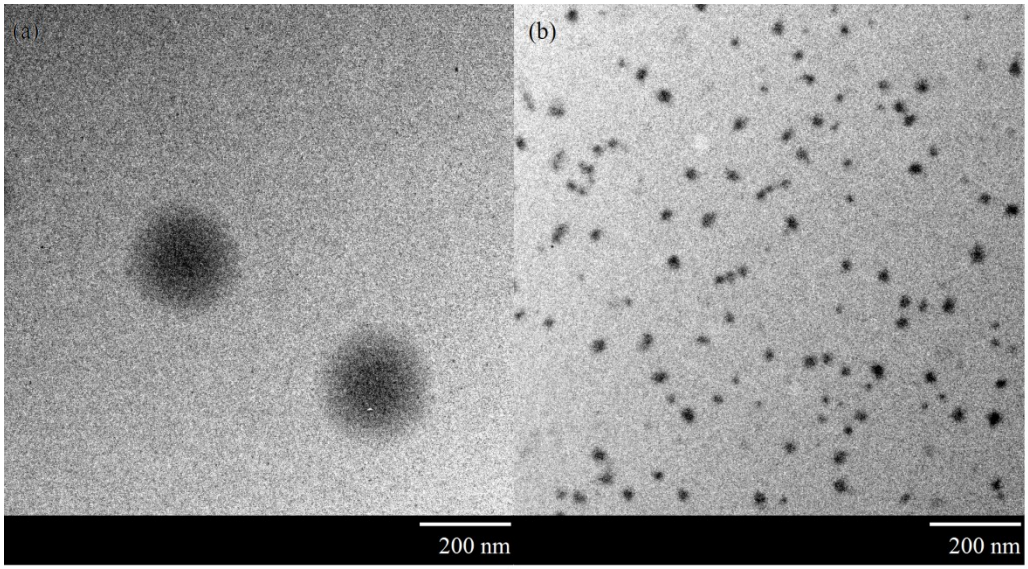

Figure S9. TEM images of the assembled micelles without and with trivalent salt before dialysis are shown in (a) and (b), respectively.

REFERENCES

1 K. Kremer, and G. S. Grest, *J. Chem. Phys.*, 1990, **92**, 5057-5086.

2 B. Dunweg, and K. Kremer, *J. Chem. Phys.*, 1993, **99**, 6983-6997.

3 U. Micka, C. Holm, and K. Kremer, *Langmuir*, 1999, **15**, 4033-4044.

4 A. Jusufi, *J. Chem. Phys.*, 2006, **124**, 044908.

5 I. C. Yeh, and M. L. Berkowitz, *J. Chem. Phys*., 1999, **111**, 3155-3162.